HHS Public Access

Author manuscript

ACS Appl Mater Interfaces. Author manuscript; available in PMC 2024 February 01.

Published in final edited form as:

ACS Appl Mater Interfaces. 2023 February 01; 15(4): 5019–5027. doi:10.1021/acsami.2c22741.

Ionic Strength and Hybridization Position Near Gold Electrodes Can Significantly Improve Kinetics in DNA-Based Electrochemical Sensors

Niamat Khuda,

Subramaniam Somasundaram,

Ajay B. Urgunde,

Christopher J. Easley*

Department of Chemistry and Biochemistry, Auburn University, Auburn, AL 36849, USA

Abstract

A variety of electrochemical (EC) biosensors play critical roles in disease diagnostics. More recently, DNA-based EC sensors have been established as promising for detecting a wide range of analyte classes. Since most of these sensors rely on the high specificity of DNA hybridization for analyte binding or structural control, it is crucial to understand the kinetics of hybridization at the electrode surface. In this work, we have used methylene blue labeled DNA (MB-DNA) strands to monitor the kinetics of DNA hybridization at the electrode surface with square-wave voltammetry (SWV). By varying the position of the double-stranded DNA (dsDNA) segment relative to the electrode surface as well as the bulk solution's ionic strength (0.125 to 1.00 M), we observed significant interferences with DNA hybridization closer to the surface, with more substantial interference at lower ionic strength. As a demonstration of the effect, toehold-mediated strand displacement reactions were slowed and diminished close to the surface, while strategic placement of the DNA binding site improved reaction rates and yields. This work manifests that both salt concentration and DNA hybridization site relative to the electrode are important factors to consider when designing DNA-based EC sensors that measure hybridization directly at the electrode surface.

Graphical Abstract

***Corresponding Author:** Professor Christopher J. Easley - Department of Chemistry and Biochemistry, Auburn University, Auburn, Alabama 36849, United States; chris.easley@auburn.edu.

Author Contributions

N.K., S.S., and C.J.E. conceived the study, designed experiments, analyzed data, and collaboratively wrote the manuscript. A.B.U. analyzed data and collaboratively wrote the manuscript. N.K. and S.S. performed experiments under the supervision of C.J.E.

Supporting Information. The Supporting Information is available free of charge at https://pubs.acs.org/.

EC_DNA_surface_kinetics_SupInfo_v08 (Microsoft Word file): This document includes a list of DNA sequences used.

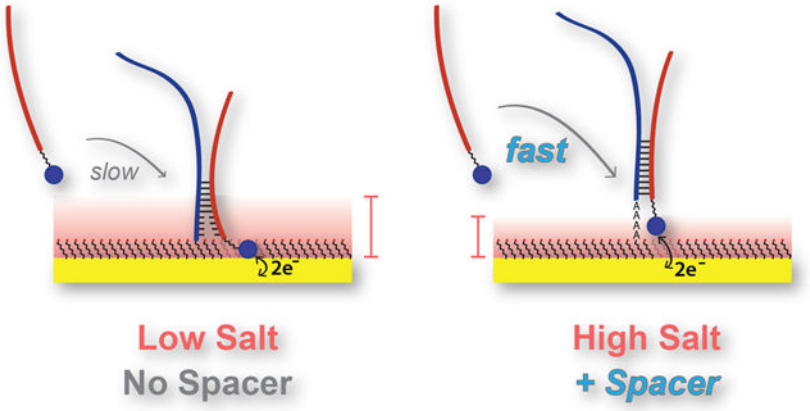

Keywords

biosensor; DNA hybridization; double-layer; surface effects; electrochemistry; square-wave voltammetry

INTRODUCTION

The development of DNA-based sensors for highly sensitive, sequence-specific quantification has become valuable due to their extensive applications in clinical diagnosis, pathogen detection, gene expression studies, and environmental monitoring.[1–4] There are numerous analytical techniques that have been established for oligonucleotide detection, such as fluorescence, electrochemistry, surface plasmon resonance, chemiluminescence, photoelectrochemistry, and quartz crystal microbalance.[5–8] Among these methods, usage of electrochemical (EC) DNA sensors has grown, owing to their reliability, rapid response, low cost, portability, lower sample requirements, their ability to work on complex/multicomponent samples, and their remarkably high sensitivity and selectivity.[9–14] Many nucleic-acid based EC sensors use structure switching probes for target-dependent signal change[15], and some of these sensors have recently made an impressive leap into real-time blood measurements in living animals.[16–20] Other sensor architectures based on steric hindrance[10, 21, 22] and tethered diffusion of surface DNA probes have been developed more recently to address generalizability.[23–27] The variety of targeted analytes have been greatly expanded[28] from the original sensors of nucleic acids to other molecular categories such as small drug molecules, small hormones, peptides, and larger proteins (e.g. antibodies) within the field of EC sensors.

Regardless of the analyte class, a common theme in these DNA-based EC sensors is a foundation made from a self-assembled monolayer (SAM) and nucleic acid as a signaling element on the electrode.[29] Along with complementary base-pair hybridization between long oligonucleotides for DNA detection, several DNA-based sensors targeting analytes employ short oligonucleotides (≤10 base pairs) toward this goal.[30–34] For example, Plaxco and co-workers have constructed a smart bioelectrochemical switch to directly quantify antibodies in blood samples. The target distorted the 5 base pair (bp) stem-

loop conformation of the probe DNA on the surface, resulting in analyte-dependent electrochemical signal change.[32]

In our previous works, we have reported a highly sensitive and selective electrochemical proximity assay (ECPA), where analyte-induced DNA hybridization (5, 7, or 10 bp) on the surface resulted in the recruitment of a redox-tagged DNA strand closer to the sensor surface.[30, 31] Several research groups have studied the performance of similar EC sensors by investigating the effects of immobilized probe structure,[35] surface density,[36] nature of the co-adsorbates,[37] redox reporters,[38] reversible cation-induced collapse,[39] nuclease hydrolysis rates,[40] and modifications in the square-wave voltammetry (SWV) frequency.[41] However, the dependence of such EC signals on the relative distance of DNA binding sites from the electrode surface has not been extensively explored. As solution-to-surface hybridization is distinct from solution-phase hybridization in terms of kinetics and thermodynamics,[42, 43] sensor performance may be sensitive to the location of the redox reporter and/or DNA binding site. The surface charge will likely alter the hybridization rate of negatively charged DNA[24, 44], thereby altering the signaling properties of the EC sensor. Especially for short hybridization sequences (≤10 bp) near the electrode surface, this effect may lead to distinctive consequences such as low binding energy and loss of assay performance.

Here, we describe a detailed study in which we varied the site of DNA hybridization relative to the electrode under different conditions. The experimental results showed that the surface hybridization kinetics of short DNA strands depend strongly upon the distance between the electrode and the binding site, and the ionic strength dependence suggests that this effect is driven by the electric double-layer. The importance of this effect is demonstrated using toehold-mediated DNA strand displacement reactions at the electrodes, where more rapid and efficient sensing is achieved by distancing the binding site away from the electrode. Ultimately, this study suggests that the position of the nucleic acid hybridization site relative to the electrode should be carefully controlled in conjunction with the bulk ionic strength when developing DNA-based EC sensors.

EXPERIMENTAL

Reagents and Materials.

All solutions were prepared with deionized, ultrafiltered water (Fisher Scientific). The following reagents were used as received: 4-(2-hydroxyethyl)-1-piperazineethanesulfonic acid (HEPES) (99.5%), tris-(2-carboxyethyl) phosphine hydrochloride (TCEP), (Sigma-Aldrich, St. Louis, MO). HPLC-purified, methylene blue-conjugated DNA (MB-DNA) was purchased from Biosearch Technologies (Novato, CA). Oligonucleotides were obtained from Integrated DNA Technologies (IDT; Coralville, Iowa). Sequences of single-stranded DNA (ssDNA) used in the experiment are given in Table S-1. These sequences were designed using the nucleic acid package webserver (NUPACK).[45]

Preparation of the Electrode.

Electrochemical sensors for the kinetics study were prepared using an Au working electrode (2 mm diameter, CH Instruments, Inc., Austin, TX). The electrodes were polished using a

previously reported protocol,[30] with slight modification. Briefly, electrodes were cleaned with freshly prepared piranha solution (H_2SO_4/H_2O_2, 3:1) for 5 min and rinsed with deionized (DI) water. To obtain a uniform surface area, electrodes were polished carefully with an aqueous alumina slurry with particle size of ~0.05 μm (Buehler, Lake Bluff, IL) for 3 min followed by sonication in ethanol/water (1:1) for 5 min. Subsequently, the Au electrode was rinsed with deionized water and electrochemically etched using cyclic voltammetry (CV) in 0.5 M H_2SO_4 by applying the potential from −0.35 to +1.5 V vs. Ag|AgCl(s) (3 M KCl) at a scan rate of 0.1 V s^{-1} for 5 cycles to remove the impurities. The cleaned Au electrode was thoroughly rinsed with DI water and dried using a stream of nitrogen gas.

DNA Self-assembled Monolayer Formation.

Typical experiments included the preparation of three electrodes in parallel, as follows. Thiolated DNA (thio-DNA), with a dithiol group at its 5' terminus, was used for monolayer assembly. The dithiol was reduced to a monothiol with TCEP to effectively form the self-assembled monolayer (SAM). A 6 μL portion (2 μL per electrode) of 200 μM thiolated DNA was mixed with 18 μL (6 μL per electrode) of 10 mM TCEP and incubated for 1 h at room temperature (~21 °C) in the dark for reduction of disulfide. The solution was then diluted to a total volume of 300 μL in HEPES/$NaClO_4$ buffer (10 mM HEPES and 0.5 M $NaClO_4$, pH 7.0; referred to herein as "buffer")[30] to a final concentration of 1.25 μM. Unless otherwise noted, all solutions used in the following experiments were carried out in buffer at pH 7.0 and 0.5 M salt. Immobilization of DNA was carried out by directly transferring freshly cleaned electrodes to the reduced thiol-DNA solution and incubating them for 1 h at room temperature in the dark. Following the self-assembled monolayer (SAM) formation, the electrodes were thoroughly rinsed with deionized water (~ 20 s) to remove any excess thio-DNA physically adsorbed on the surface. To prevent nonspecific binding, the SAM-modified electrode was immediately transferred to 3 mM 6-mercaptohexanol (MCH) solution and incubated for 1 h at room temperature in the dark[46] followed by gentle rinsing with DI water (~ 40 s) to remove any excess MCH. The electrode was then placed into a glass container with buffer until ready for use.

Electrochemical Measurements.

Electrochemical measurements were performed using a GAMRY Reference 600 electrochemical workstation with a standard three-electrode system composed of an Ag|AgCl(s) (3 M KCl) reference electrode (Bioanalytical Systems), Pt wire counter electrode, and an Au as a working electrode (diameter = 2 mm). All potentials are reported relative to Ag|AgCl (3 M KCl) reference electrode. Electrochemical measurements were performed at 25 °C in buffer using square wave voltammetry (SWV) with a step size of 1 mV, a pulse height of 25 mV, and a frequency of 100 Hz over the potential range from −0.45 to 0 V (average of −0.225 V). For the hybridization kinetics measurements, a voltammetric trace was recorded upon immersion of the electrode into the sample ($t \approx 0$ min), and a scan was carried out every 5 min for 125 min. For the calibration experiment, the sensor was allowed to equilibrate in 500 μL of buffer with various concentrations of M10 DNA for 30 min at 25 °C. Subsequently, the counter and reference electrodes were introduced, and SWV measurement was initiated.

Hybridization Kinetics.

The sensor was immersed in a glass electrochemical cell containing 100 nM MB conjugated DNA sequences (M10 DNA) in 500 μL of buffer to study the binding kinetics of a short (10 bp) DNA hybridization segment. For varying the double-layer thicknesses, four different salt concentrations were used to prepare the buffer solutions: 0.125 M, 0.25 M, 0.5 M, and 1.0 M $NaClO_4$. As a control experiment, M40 DNA in 0.5 M $NaClO_4$ was used to increase the number and stability of complementary bases (40 bp), since this long complementary strand's stability should not be significantly affected by the double layer. For toehold-mediated strand displacement studies, two competitor DNA sequences (C-33-LTH and C-33-UTH), were used as shown in Table S-1. The sensor was allowed to equilibrate with 500 nM of competitor in 300 μL buffer for 24 h at room temperature (~21 °C) in the dark. Following the duplex formation of competitor and thio-DNA, the electrodes were rinsed with buffer (~ 5 s) to remove any excess physically adsorbed competitor from the surface. To initiate strand displacement and study the role of hybridization site, the sensor was incubated in 100 nM of M40 DNA in 500 μL of buffer. For all kinetics studies, SWV measurements were made once every 5 min.

Data Analysis.

For all experiments, each set of raw SWV data (including V_{step} and I_{diff} data) was transferred to Microsoft Excel, and a third-order polynomial baseline was calculated near the redox potential of MB-DNA. The "Linest" function in Excel was used, and data points from −0.450 to −0.360 V and −0.12 to −0.001 V were selected for baseline fitting. The baseline function was subtracted from the raw data to get a baseline-corrected SWV voltammogram. The maximum current from this graph was used as the peak height of each particular run. Additional details are provided in our previous work.[27]

In studying hybridization kinetics, the reversible DNA–DNA hybridization on the electrode surface can be described by a Langmuir kinetic model,[47]

$$\frac{d\theta}{dt} = k_{on}c(1 - \theta) - k_{off}\theta \quad (1)$$

Where θ is the fraction of hybridized target DNA on the surface, c is the concentration of target ssDNA in solution, and k_{on} and k_{off} are the association and dissociation rate constants, respectively. The solution of this first-order differential equation is,

$$\theta = \frac{K_c}{1 + K_c}(1 - e^{-\frac{t}{\tau}}) \quad (2)$$

The equation describes the adsorption kinetics, where $K_c = k_{on} / k_{off}$ is the equilibrium constant. Figure S-1 in Supporting Information shows a normalized and log-transformed version of Equation 2 which was used to fit kinetic data and estimate the hybridization time constant, τ, a constant that provides the time (in minutes) required to reach ~63% of the asymptotic equilibrium value. This time constant (i.e. the lifetime of the process) is related to the rate constants as follows.

$$\tau = \frac{1}{k_{on} + k_{off}} \quad (3)$$

Hybridization data were analyzed in GraphPad Prism 7.03. For all determinations of hybridization time constant, τ, the average of three kinetic measurements with three different electrodes was used, plugged into Equation S-1, then linearly fit to determine τ; error bars on lifetime values represent standard errors after the slope determination from the linear fit.

RESULTS AND DISCUSSION

Hybridization of short DNA strands near the electrode surface.

Electrochemical assays based on DNA hybridization have been expanded by successfully quantifying a wide range of analytes in the past decade.[5, 13, 25, 27, 28, 32] The unique flexibility in DNA design allows users to control the specific hybridization site and location of the redox label(s). Nonetheless, surface-based hybridization reactions are seldomly studied under assay-relevant conditions, thus there is a need for an improved understanding, particularly with shorter hybridization segments. In this work, we have evaluated sensors with a single DNA hybridization site, in which a redox-labeled ssDNA analyte in solution hybridizes to a SAM of complementary ssDNA on the electrode surface. This hybridization places the redox molecule at various, controlled distances from the electrode surface, where we use distance units of equivalent nucleotides of ssDNA (nt) for ease of understanding; a distance of 0.68 nm is considered equivalent to 1 nt.[48] Herein we designed eight different thio-DNA (0A-thiol to 7A-thiol), which places the DNA binding site at varying distances relative to the sensor surface (about 1 to 6 nm for the closest part of binding site) by tuning the length of the spacer, a series of adenines (A) at the 5’-end of thio-DNA. Nucleotides were removed from the 3’-end to preserve the length of all eight thio-DNAs at 40 nt and to promote equivalent biophysical characteristics such as flexibility and tethered diffusion. The DNA hybridization site between thio-DNAs and analyte strand M10 formed 10 base pairs (bp). The hybridization of the M40 strand formed 40 bp, which was used as a control strand which could largely avoid surface effects.

Figure 1 depicts the experimental design employed to study the kinetics of DNA hybridization (short segments of 10 bp) at different sites relative to the electrode. As the system approaches binding equilibrium, hybridization of the thio-DNA (blue) and M10 redox-labeled DNA (red) brings the MB label close enough to the Au electrode surface to enable the transfer of electrons, which leads to a faradaic electrochemical signal during the SWV potential scan. An increase in current was observed upon the addition of analyte DNA (M10), and peak currents and kinetic data were used to determine the time constants for DNA hybridization at different spacings and salt concentrations. As discussed further below, binding sites closer to the electrode and at lower ionic strengths exhibited significantly slower hybridization rates and diminished currents, likely due to double-layer interference with the base pairing interactions. Figure 1 (lower plots) also shows the expected peak currents observed over time in kinetic experiments. It is important to note that two convoluted effects will be observed, labeled with numbered circles in the figure: 1) DNA hybridization kinetics and equilibria and 2) distance dependent electron transfer. While an

intermediate spacer should allow faster hybridization and higher current, longer spacers will avoid surface effects but will exhibit lower current due to the distance from the surface.

Steady-state experiments.

In earlier steady-state measurements, we had expected the highest faradaic currents to be observed with the DNA hybridization segment and MB label closest to the surface (0 nt spacer; 0A-thiol strand). However, we consistently observed the steady-state peak currents to gradually *increase* from about 600 to 900 nA as the label was moved away from the surface, from 0 nt to about 5 nt (Figure 2a). The more precipitous decrease at distances further from the electrode (6–7 nt) was expected, since the MB label was being positioned further away. To better understand the loss of current close to the electrode, we elected to more closely study the DNA hybridization kinetics. Since this steady-state peak current loss near the electrode was not observed with long, stable DNA hybridizations (e.g. M40) in control experiments, the electric double-layer (shaded in red in Figure 1 and Figure 2a) was surmised to play a meaningful role in shorter segment hybridizations (e.g. M10).

Hybridization kinetics.

Initial kinetic experiments at different spacer lengths (Figure 2b) showed a similar effect, suggesting double-layer interference in hybridization near the surface. The 0 nt spacer exhibited the slowest observed hybridization, positioned closest to the electrode (0A-thiol, red data), as suggested by the schematic in Figure 1. As seen in Figure 2b, once the hybridized segment was spaced at least 4 nt away (4A-thiol, blue data), the rate was faster, and the system reached higher steady-state currents. Although the steady-state current was lower with longer spacers (7A-thiol, gray data), the hybridization rate was essentially equivalent to that of intermediate spacers, indicating that a surface effect was interfering with hybridization of the short DNA segment. As shown in Figure 2b, the same effect was easily observed at both 0.500 M (left) and 0.250 M (right) salt concentrations. Normalized current data (inset plots) show clearly that using a 0 nt spacer (red data) resulted in the slowest DNA hybridizations. The inset table describes the two convoluted effects (numbered in Figure 1), where current increases as the MB label is positioned closer to the electrode surface, yet DNA hybridization is impeded closer to the surface.

Double-layer thickness considerations.

At the electrode surface, it is well-known that an electric double-layer forms when exposed to a fluid such as an aqueous buffer solution.[49] The thickness of the double layer depends on the electrolyte concentration, and its thickness is related to the κ^{-1}, the Debye-Hückel length.[50]

$$\kappa^{-1} = \sqrt{\frac{\varepsilon\varepsilon_0 kT}{2n^0 z^2 e^2}} \approx \frac{3.04 \times 10^{-8}}{z\sqrt{C}} \quad (4)$$

Here ε is the relative permittivity of the solvent, ε_0 is the vacuum permittivity, k is the Boltzmann constant, T is the temperature, C is the bulk electrolyte concentration, z is the ion charge, and e is the elementary charge. Using the simplified form of Equation 4 (right), as described by Bard and Faulkner,[49] we calculated the values of the Debye-Hückel length

for the varying salt concentrations used in this study. Here, we define the value $d = 2.3 \times \kappa^{-1}$ to represent a distance at which the electrical potential decays from the surface value by 90%. For $NaClO_4$ concentrations of 1.0 M, 0.5 M, 0.25 M, and 0.125 M, we calculated the d values to be approximately 0.7 nm, 1.0 nm, 1.4 nm, and 2.0 nm, respectively. Thus, we could vary the double-layer thicknesses and control the range at which hybridization interferences may occur from 0.7 to 2.0 nm.

It should be noted that the chemical structure at our gold electrodes includes a DNA monolayer that is filled in with a protective MCH monolayer, both layers being coadsorbed,[51] and we can assume the MCH monolayer to be approximately 1.2 nm in thickness[52] based on a tilt angle of ~30° (depicted this way in Figure 1). From thickness and capacitance measurements,[53] it is understood that the MCH layer acts as a thin dielectric, yet it is also somewhat permeable to ions and has been observed to oscillate in thickness by about 0.1 nm.[54] With our particular system, double-layer calculations via Equation 4 do not consider these structural complexities, although we do know that there is significant charge on equivalent gold-MCH/DNA surfaces in buffer at floating potential.[51] Herein, we have assumed the double-layer effects calculated from Equation 4 to extend from the top of the MCH monolayer, which may limit our precision by ~1 nm (about 1 nt spacer length). Nonetheless, our results indicate that double-layer effects are most likely the cause of the hybridization interferences, as described within this work. An interesting avenue for future work would be to carry out dynamic simulations of the gold-MCH/DNA surfaces.

Effects of position and ionic strength on current and hybridization time constant.

Useful preliminary information was obtained from steady-state and kinetic measurements shown in Figure 2a–b. While steady-state peak current magnitudes can vary with electrode-to-electrode differences,[13] hybridization time constants are independent of these variations. The next study was a more thorough evaluation of similar kinetic data at varying distances from the surface (0 to 7 nt spacers) and at different ionic strengths (0.125 to 1.00 M). From these data, we calculated the maximum currents using a simple spreadsheet function, and we determined the hybridization time constants, τ, by fitting temporal data to Equation 2 (Figure 2c–d) using the transformation in Equation S-1. These experiments included 40 different experimental conditions carried out in triplicate, thus 120 different electrodes were used to obtain the data in Figure 2d.

The maximum peak current data are shown in Figure 2c. It should be noted that with increasing salt concentration, DNA binding energy is known to increase. This could have been a plausible cause of an increase in maximum current, although the effect should be the same for all eight spacer lengths tested. However, we found that the 10-bp binding at both 6 nt and 7 nt spacer lengths gave statistically the same current response ($p>0.6$) with 0.5 M and 1.0 M salt, whereas, shorter spacer lengths gave a distinct current response ($p<0.05$), indicating that the attenuation of the double-layer is most likely responsible for the improved current response for 0 to 5 nt spacers. As a control experiment, strands with much more stable hybridization energy (40 bp) were evaluated at 0.5 M ionic strength (blue data), since the dsDNA of 40 bp strands should not be significantly affected by the double layer. In this case, the fact that the current continued to increase as the MB label was positioned

closer to the electrode suggests that the very strong hybridization was able to overcome any double-layer interference effects, and the expected increasing SWV current response was observed as the MB label was moved closer to the surface.

Hybridization time constant data are shown in Figure 2d; note the logarithmic y-axis scaling. As anticipated, higher ionic strength (1.00 M) reduced double-layer effects and resulted in the shorter hybridization time constants (~10–20 min) at all spacer lengths, while lower ionic strength (0.125 M) gave pronounced double-layer effects and much longer time constants (~2–3 h). The observed strong enhancement in hybridization speed with increasing salt concentration indicated that double-layer effects could be reduced experimentally, in turn facilitating more efficient hybridization of complementary DNA close to the sensor surface. The kinetic data at the middle range of salt concentrations (0.25 and 0.5 M) provide more evidence for the same. Increasing distance from the electrode (0 to 7 nt spacers) facilitated faster kinetics in both cases. Again, the 40 bp strands were used as a control at 0.5 M ionic strength (blue data). This result essentially provided a limit on the speed of hybridization (~10–15 min time constant), and as expected, the 10-bp binding at the highest salt concentration (1.0 M; yellow data) was very similar to this control.

Structural justification of double-layer effects.

Considering the experimental evidence to this point, the depiction of the electrode surface in Figure 1 can be revisited. In this figure, the MCH monolayer was shown with a thickness of about 1.2 nm and with individual MCH molecules at a 30° tilt angle, as described in detail by others.[52] We have attempted to show the double-layer thickness (red shaded region) in the figure to scale, compared to the MCH monolayer thickness, the 4-nt spacer length, the 10-bp segment of dsDNA, and the MB-to-DNA tether length. For clarity, all these molecular lengths are shown in the fully extended polymer conformation, therefore it is probable that the average lengths are shorter than we depicted. The double-layer is shown as if the ionic strength were 0.5 M, giving $d = 2.3 \times \kappa^{-1} \approx 1.0$ nm. It is clear from Figure 1a (right) that with no spacer included in the thio-DNA (0A-thiol), the double-layer has the propensity to interfere with several of the DNA base pairs within the 10-bp segment of the dsDNA (M10 bound to 0A-thiol). This effect would destabilize DNA binding, causing slowed hybridization kinetics, and it would be ionic strength dependent, all of which agree with our experimental observations (Figure 2). By contrast, when we include at least a 4 nt spacer, the dsDNA is physically cleared from significant interactions with the double-layer, particularly in its fully extended form as shown in Figure 1b (right). The spacer would thus promote typical (faster) hybridization rates at longer distance and higher ionic strength, as observed in experiments.

Toehold-mediated strand displacement near electrode surfaces.

A useful demonstration of the observed double-layer effects is provided by positioning short DNA hybridization sites near or far from the electrode surface. Toehold-mediated strand displacement reactions using DNA[55, 56] have become increasingly important in binding reactions used in analytical chemistry, bioanalysis, and nanotechnology. These systems typically rely on a short, ssDNA toehold segment or domain that facilitates displacement of a larger, dsDNA domain within the same strand; the displacement is initiated by an

invading strand complementary to the ssDNA domain and part of the dsDNA domain sequence. Here, we built a mock sensor using the 40 nt DNA strand (M40) as the analyte (i.e. invading strand) to bind to a 7 nt toehold, thereby triggering strand displacement of a 33 bp competitor hybridized to thio-DNA at the gold electrode surface (Figure 3a–b). Two competitor DNA sequences were designed (C-33-LTH and C-33-UTH in Table S-1), in such a way that they expose either a lower toehold (LTH) or an upper toehold (UTH). The LTH is positioned close to the electrode, while the UTH is far from the electrode. As shown in the schematic, the kinetics of hybridization to an LTH (Figure 3a) should be significantly slower than binding to a UTH (Figure 3b). In both cases, the M40-to-thio-DNA binding energies are equal (40 bp) and larger than the competitor-to-thio-DNA energies (33 bp), and the toeholds are of equal length (7 nt), such that toehold mediated strand displacement should be equally favored in both systems unless the toehold position relative to the electrode is relevant.

As shown in Figure 3c–d, the M40 strand readily displaced the competitor strand when the toehold was not near the surface (UTH; light blue). Hybridization time constants for UTH systems were short ($\tau \approx 15$–22 min), even approaching that of the 40 bp control experiments (red, blue; rightmost data) that did not include a competitor strand ($\tau \approx 11$–16 min). By contrast, the lower toehold systems (LTH; green) showed obvious interference from double-layer effects, which slowed hybridization kinetics significantly ($\tau \approx 34$–39 min). The impeded access of the analyte or invading strand (M40) to the LTH also reduced the asymptotic peak current when nearest to the surface (0 nt spacer; leftmost data). While the LTH system with a 4 nt spacer (green; middle data) was noticeably slower, it appears that the spacer gave the strand displacement reaction enough stability to eventually (> 2 h) approach steady-state currents that were comparable to the UTH system.

The 40 bp control experiments (red, blue; rightmost data) did not include a competitor strand, and by inference no toehold. In this instance, unimpeded 40-bp hybridization with the surface strand was not only more thermodynamically stable than the 33-bp hybridizations, but the lack of a toehold or competitor strand promoted faster hybridization as well. In this case, the equilibrium should be expected to be shifted further toward surface binding without a competitor, the kinetics should be fast without the competitor, and the steady-state currents should be higher by comparison. The data in Figure 3d matched with all of these expectations. Yet another interesting finding emerged from these data. Even though 40 bp binding is highly stable, the hybridization kinetics without a surface spacer were still somewhat impeded ($\tau \approx 16$ min) by the double-layer compared to that with a 4 nt spacer ($\tau \approx 11$ min). These data suggest that hybridization of even longer strands could be affected by the double-layer, albeit to a lesser extent.

Improving response of DNA-based EC sensors.

Finally, to further demonstrate the importance of controlling position and bulk ionic strength in DNA-based EC systems, we designed an E-DNA sensor[57] with both favorable and unfavorable conditions of ionic strength and hybridization site positioning relative to the electrode. The peak height current plot of different analyte (M10) concentrations ranging from 1 nM to 160 nM is presented in Figure 4. It was observed that for a 4 nt spacer

(4A-thiol) with 1.00 M ionic strength, the peak current increased in proportion to the concentration of analyte, resulting in a curve that fits well to a Langmuir isotherm (blue curve). Data at low concentrations show good linearity (inset) in the range of 1 to 40 nM ($R^2 = 0.979$); the sensitivity (slope of the best fit linear equation) was 14.0 nA nM^{-1}, and the 3σ LOD for M10 DNA was 300 pM. By contrast, with no spacer (0A-thiol) and at 0.125 M ionic strength, the sensitivity of the E-DNA sensor was only 0.0719 nA nM^{-1}, and the LOD was much worse at 40 nM. The sensitivity improvement with a 4 nt spacer at high ionic strength compared to no spacer at low ionic strength was ~190-fold, and the LOD was improved by ~130-fold. These results, with drastically improved LOD and sensitivity, indicate that salt concentration and hybridization sites are important parameters that should be considered in sensor design. These findings should also allow users to engineer improved versions of previously developed E-DNA sensors.

CONCLUSIONS

Since DNA plays a vital role in the E-DNA class of biosensors and various other modern electrochemical sensors, an improved understanding of the kinetics of DNA hybridization at the electrode surface is crucial. Unlike in solution-based hybridization, we found surface binding kinetics to depend strongly on the distance between the electrode and the DNA binding site. As the site was positioned closer to the surface, decreases in hybridization kinetics were observed, implicating the electric double-layer as interfering with hybridization. Indeed, reduction of double-layer thickness with high ionic strength increased kinetics near the surface, and lower salt concentrations decreased kinetics, even at more distant sites. Strategically designed DNA strand displacement reactions at electrodes further validated our findings. Using toehold sites close to the electrode diminished the reaction speed and yield, while sites further from the electrode—with the same number of base pairs—showed faster and more efficient binding. Interestingly, we also showed that hybridization of even longer strands could be moderately affected by the double-layer. This work has important implications in DNA-based biosensors, showing that the positions of nucleic acid hybridization sites relative to the electrode, as well as the bulk ionic strength, should be carefully chosen in each system.

Supplementary Material

Refer to Web version on PubMed Central for supplementary material.

Funding Sources

Research reported in this manuscript was supported by the National Institute of General Medical Sciences (NIGMS) of the National Institutes of Health (NIH) under award number R01 GM138828. The content of this manuscript is solely the responsibility of the authors and does not necessarily represent the official views of the NIH.

REFERENCES

(1). Xiong E; Zhang X; Liu Y; Zhou J; Yu P; Li X; Chen J Ultrasensitive electrochemical detection of nucleic acids based on the dual-signaling electrochemical ratiometric method and exonuclease III-assisted target recycling amplification strategy. Anal. Chem 2015, 87 (14), 7291–7296. [PubMed: 26125332]

(2). Liu J; Cao Z; Lu Y Functional Nucleic Acid Sensors. Chem. Rev 2009, 109 (5), 1948–1998. DOI: 10.1021/cr030183i. [PubMed: 19301873]

(3). Lu CH; Yang HH; Zhu CL; Chen X; Chen GN A graphene platform for sensing biomolecules. Angew. Chem 2009, 121 (26), 4879–4881.

(4). Sawyers CL The cancer biomarker problem. Nature 2008, 452 (7187), 548–552. [PubMed: 18385728]

(5). Smith SJ; Nemr CR; Kelley SO Chemistry-Driven Approaches to Ultrasensitive Nucleic Acid Detection. J. Am. Chem. Soc 2016.

(6). Sassolas A; Leca-Bouvier BD; Blum LJ DNA biosensors and microarrays. Chem. Rev 2008, 108 (1), 109–139. [PubMed: 18095717]

(7). Li Y; Zeng R; Wang W; Xu J; Gong H; Li L; Li M; Tang D Size-Controlled Engineering Photoelectrochemical Biosensor for Human Papillomavirus-16 Based on CRISPR-Cas12a-Induced Disassembly of Z-Scheme Heterojunctions. ACS Sens. 2022, 7 (5), 1593–1601. DOI: 10.1021/acssensors.2c00691. [PubMed: 35510603]

(8). Zeng R; Gong H; Li Y; Li Y; Lin W; Tang D; Knopp D CRISPR-Cas12a-Derived Photoelectrochemical Biosensor for Point-Of-Care Diagnosis of Nucleic Acid. Anal. Chem 2022, 94 (20), 7442–7448. DOI: 10.1021/acs.analchem.2c01373. [PubMed: 35549163]

(9). Wang H; Wang Y; Liu S; Yu J; Guo Y; Xu Y; Huang J Signal-on electrochemical detection of antibiotics based on exonuclease III-assisted autocatalytic DNA biosensing platform. RSC Adv. 2016, 6 (49), 43501–43508.

(10). Mahshid SS; Camiré S b.; Ricci, F.; Vallée-Bélisle, A. A highly selective electrochemical DNA-based sensor that employs steric hindrance effects to detect proteins directly in whole blood. J. Am. Chem. Soc 2015, 137 (50), 15596–15599. [PubMed: 26339721]

(11). Lubin AA; Plaxco KW Folding-based electrochemical biosensors: the case for responsive nucleic acid architectures. Acc. Chem. Res 2010, 43 (4), 496–505. [PubMed: 20201486]

(12). Hianik T; Wang J Electrochemical aptasensors–recent achievements and perspectives. Electroanalysis 2009, 21 (11), 1223–1235.

(13). Pellitero MA; Shaver A; Arroyo-Currás N Critical Review—Approaches for the Electrochemical Interrogation of DNA-Based Sensors: A Critical Review. J. Electrochem. Soc 2020, 167 (3), 037529. DOI: 10.1149/2.0292003jes.

(14). Lv H; Chen A; Cheng W; Kong L; Zhao M; Ding S; Ju H; Cheng W Efficient DNA Walker Guided with Well-Regulated Interfacial Tracks for Ultrasensitive Electrochemiluminescence Biosensing. Anal. Chem 2020, 92 (23), 15624–15631. DOI: 10.1021/acs.analchem.0c03893. [PubMed: 33170673]

(15). Schoukroun-Barnes LR; Macazo FC; Gutierrez B; Lottermoser J; Liu J; White RJ Reagentless, Structure-Switching, Electrochemical Aptamer-Based Sensors. Annu. Rev. Anal. Chem. (Palo Alto Calif) 2016, 9 (1), 163–181. DOI: 10.1146/annurev-anchem-071015-041446 From NLM. [PubMed: 27070185]

(16). Arroyo-Currás N; Somerson J; Vieira PA; Ploense KL; Kippin TE; Plaxco KW Real-time measurement of small molecules directly in awake, ambulatory animals. Proc. Natl. Acad. Sci. USA 2017, 114 (4), 645. DOI: 10.1073/pnas.1613458114. [PubMed: 28069939]

(17). Li H; Li S; Dai J; Li C; Zhu M; Li H; Lou X; Xia F; Plaxco Kevin W. High frequency, calibration-free molecular measurements in situ in the living body. Chem. Sci 2019, 10 (47), 10843–10848, 10.1039/C9SC04434E. DOI: 10.1039/C9SC04434E. [PubMed: 34040713]

(18). Scida K; Plaxco KW; Jamieson BG High frequency, real-time neurochemical and neuropharmacological measurements in situ in the living body. Transl. Res 2019, 213, 50–66. DOI: 10.1016/j.trsl.2019.07.004. [PubMed: 31361988]

(19). Arroyo-Currás N; Dauphin-Ducharme P; Scida K; Chávez JL From the beaker to the body: translational challenges for electrochemical, aptamer-based sensors. Anal. Methods 2020, 12 (10), 1288–1310, 10.1039/D0AY00026D. DOI: 10.1039/D0AY00026D.

(20). Wu Y; Tehrani F; Teymourian H; Mack J; Shaver A; Reynoso M; Kavner J; Huang N; Furmidge A; Duvvuri A; et al. Microneedle Aptamer-Based Sensors for Continuous, Real-Time Therapeutic Drug Monitoring. Anal. Chem 2022, 94 (23), 8335–8345. DOI: 10.1021/acs.analchem.2c00829 From NLM Medline. [PubMed: 35653647]

(21). Mahshid SS; Vallée-Bélisle A; Kelley SO Biomolecular Steric Hindrance Effects Are Enhanced on Nanostructured Microelectrodes. Anal. Chem 2017, 89 (18), 9751–9757. DOI: 10.1021/acs.analchem.7b01595. [PubMed: 28829912]

(22). Zhou W; Mahshid SS; Wang W; Vallée-Bélisle A; Zandstra PW; Sargent EH; Kelley SO Steric Hindrance Assay for Secreted Factors in Stem Cell Culture. ACS Sens. 2017, 2 (4), 495–500. DOI: 10.1021/acssensors.7b00136. [PubMed: 28723184]

(23). Knezevic J; Langer A; Hampel PA; Kaiser W; Strasser R; Rant U Quantitation of Affinity, Avidity, and Binding Kinetics of Protein Analytes with a Dynamically Switchable Biosurface. J. Am. Chem. Soc 2012, 134 (37), 15225–15228. DOI: 10.1021/ja3061276. [PubMed: 22946661]

(24). Rant U; Arinaga K; Fujita S; Yokoyama N; Abstreiter G; Tornow M Dynamic Electrical Switching of DNA Layers on a Metal Surface. Nano Lett. 2004, 4 (12), 2441–2445. DOI: 10.1021/nl0484494.

(25). Somasundaram S; Easley CJ A Nucleic Acid Nanostructure Built through On-Electrode Ligation for Electrochemical Detection of a Broad Range of Analytes. J. Am. Chem. Soc 2019, 141 (29), 11721–11726. DOI: 10.1021/jacs.9b06229. [PubMed: 31257869]

(26). Das J; Gomis S; Chen JB; Yousefi H; Ahmed S; Mahmud A; Zhou W; Sargent EH; Kelley SO Reagentless biomolecular analysis using a molecular pendulum. Nat. Chem 2021, 13 (5), 428–434. DOI: 10.1038/s41557-021-00644-y From NLM Medline. [PubMed: 33686229]

(27). Khuda N; Somasundaram S; Easley CJ Electrochemical Sensing of the Peptide Drug Exendin-4 Using a Versatile Nucleic Acid Nanostructure. ACS Sens. 2022, 7 (3), 784–789. DOI: 10.1021/acssensors.1c02336 From NLM Medline. [PubMed: 35180342]

(28). Parolo C; Idili A; Ortega G; Csordas A; Hsu A; Arroyo-Currás N; Yang Q; Ferguson BS; Wang J; Plaxco KW Real-Time Monitoring of a Protein Biomarker. ACS Sens. 2020, 5 (7), 1877–1881. DOI: 10.1021/acssensors.0c01085. [PubMed: 32619092]

(29). Shaver A; Curtis SD; Arroyo-Currás N Alkanethiol Monolayer End Groups Affect the Long-Term Operational Stability and Signaling of Electrochemical, Aptamer-Based Sensors in Biological Fluids. ACS Appl. Mater. Interfaces 2020, 12 (9), 11214–11223. DOI: 10.1021/acsami.9b22385. [PubMed: 32040915]

(30). Hu J; Wang T; Kim J; Shannon C; Easley CJ Quantitation of femtomolar protein levels via direct readout with the electrochemical proximity assay. J. Am. Chem. Soc 2012, 134 (16), 7066–7072. [PubMed: 22452720]

(31). Hu J; Yu Y; Brooks JC; Godwin LA; Somasundaram S; Torabinejad F; Kim J; Shannon C; Easley CJ A reusable electrochemical proximity assay for highly selective, real-time protein quantitation in biological matrices. J. Am. Chem. Soc 2014, 136 (23), 8467–8474. [PubMed: 24827871]

(32). Vallée-Bélisle A; Ricci F; Uzawa T; Xia F; Plaxco KW Bioelectrochemical switches for the quantitative detection of antibodies directly in whole blood. J. Am. Chem. Soc 2012, 134 (37), 15197–15200. [PubMed: 22913425]

(33). Zhang H; Li X-F; Le XC Binding-induced DNA assembly and its application to yoctomole detection of proteins. Anal. Chem 2011, 84 (2), 877–884. [PubMed: 22239834]

(34). Liu S; Fang L; Wang Y; Wang L Universal Dynamic DNA Assembly-Programmed Surface Hybridization Effect for Single-step, Reusable, and Amplified Electrochemical Nucleic Acid Biosensing. Anal. Chem 2017.

(35). White RJ; Plaxco KW Engineering New Aptamer Geometries for Electrochemical Aptamer-Based Sensors. Proc. SPIE 2009, 7321, 732105. DOI: 10.1117/12.820419 PMC.

(36). White RJ; Phares N; Lubin AA; Xiao Y; Plaxco KW Optimization of Electrochemical Aptamer-Based Sensors via Optimization of Probe Packing Density and Surface Chemistry. Langmuir 2008, 24 (18), 10513–10518. DOI: 10.1021/la800801v PMC. [PubMed: 18690727]

(37). Ricci F; Zari N; Caprio F; Recine S; Amine A; Moscone D; Palleschi G; Plaxco KW Surface chemistry effects on the performance of an electrochemical DNA sensor. Bioelectrochemistry 2009, 76 (0), 10.1016/j.bioelechem.2009.1003.1007. DOI: 10.1016/j.bioelechem.2009.03.007 PMC.

(38). Kang D; Ricci F; White RJ; Plaxco KW Survey of Redox-Active Moieties for Application in Multiplexed Electrochemical Biosensors. Anal. Chem 2016, 88 (21), 10452–10458. [PubMed: 27659949]

(39). Sykes KS; Oliveira LFL; Stan G; White RJ Electrochemical Studies of Cation Condensation-Induced Collapse of Surface-Bound DNA. Langmuir 2019, 35 (40), 12962–12970. DOI: 10.1021/acs.langmuir.9b02299. [PubMed: 31509702]

(40). Shaver A; Kundu N; Young BE; Vieira PA; Sczepanski JT; Arroyo-Curras N Nuclease Hydrolysis Does Not Drive the Rapid Signaling Decay of DNA Aptamer-Based Electrochemical Sensors in Biological Fluids. Langmuir 2021, 37 (17), 5213–5221. DOI: 10.1021/acs.langmuir.1c00166 From NLM Medline. [PubMed: 33876937]

(41). Dauphin-Ducharme P; Plaxco KW Maximizing the Signal Gain of Electrochemical-DNA Sensors. Anal. Chem 2016, 88 (23), 11654–11662. [PubMed: 27805364]

(42). Gao Y; Wolf LK; Georgiadis RM Secondary structure effects on DNA hybridization kinetics: a solution versus surface comparison. Nucleic Acids Res. 2006, 34 (11), 3370–3377. [PubMed: 16822858]

(43). Fish DJ; Horne MT; Brewood GP; Goodarzi JP; Alemayehu S; Bhandiwad A; Searles RP; Benight AS DNA multiplex hybridization on microarrays and thermodynamic stability in solution: a direct comparison. Nucleic Acids Res. 2007, 35 (21), 7197–7208. [PubMed: 17947320]

(44). Vainrub A; Montgomery Pettitt B Surface electrostatic effects in oligonucleotide microarrays: control and optimization of binding thermodynamics. Biopolymers 2003, 68 (2), 265–270. [PubMed: 12548628]

(45). Zadeh JN; Steenberg CD; Bois JS; Wolfe BR; Pierce MB; Khan AR; Dirks RM; Pierce NA NUPACK: analysis and design of nucleic acid systems. J. Comput. Chem 2011, 32 (1), 170–173. [PubMed: 20645303]

(46). Xiao Y; Lai RY; Plaxco KW Preparation of electrode-immobilized, redox-modified oligonucleotides for electrochemical DNA and aptamer-based sensing. Nat. Protoc 2007, 2 (11), 2875–2880. [PubMed: 18007622]

(47). Fiche JB; Buhot A; Calemczuk R; Livache T Temperature Effects on DNA Chip Experiments from Surface Plasmon Resonance Imaging: Isotherms and Melting Curves. Biophys. J 2007, 92 (3), 935–946. DOI: 10.1529/biophysj.106.097790. [PubMed: 17085497]

(48). Chi Q; Wang G; Jiang J The persistence length and length per base of single-stranded DNA obtained from fluorescence correlation spectroscopy measurements using mean field theory. Physica A 2013, 392 (5), 1072–1079. DOI: 10.1016/j.physa.2012.09.022.

(49). Bard AJ; Faulkner LR Electrochemical methods: fundamentals and applications, 2nd ed.; Wiley: Hoboken, N. J.,, 2001.

(50). Stojek Z The electrical double layer and its structure. In Electroanalytical methods, Springer-Verlag Berlin Heidelberg, 2010; pp 3–9.

(51). Arinaga K; Rant U; Tornow M; Fujita S; Abstreiter G; Yokoyama N The Role of Surface Charging during the Coadsorption of Mercaptohexanol to DNA Layers on Gold: Direct Observation of Desorption and Layer Reorientation. Langmuir 2006, 22 (13), 5560–5562. DOI: 10.1021/la060324m. [PubMed: 16768474]

(52). Bain CD; Troughton EB; Tao YT; Evall J; Whitesides GM; Nuzzo RG Formation of monolayer films by the spontaneous assembly of organic thiols from solution onto gold. J. Am. Chem. Soc 1989, 111 (1), 321–335. DOI: 10.1021/ja00183a049.

(53). Sondag-Huethorst JAM; Fokkink LGJ Electrochemical Characterization of Functionalized Alkanethiol Monolayers on Gold. Langmuir 1995, 11 (6), 2237–2241. DOI: 10.1021/la00006a062.

(54). Hiasa T; Onishi H Mercaptohexanol assembled on gold: FM-AFM imaging in water. Colloids Surf. A: Physicochem. Eng 2014, 441, 149–154. DOI: 10.1016/j.colsurfa.2013.09.002.

(55). Zhang DY; Winfree E Control of DNA Strand Displacement Kinetics Using Toehold Exchange. J. Am. Chem. Soc 2009, 131 (47), 17303–17314. DOI: 10.1021/ja906987s. [PubMed: 19894722]

(56). Li F; Tang Y; Traynor SM; Li X-F; Le XC Kinetics of Proximity-Induced Intramolecular DNA Strand Displacement. Anal. Chem 2016, 88 (16), 8152–8157. DOI: 10.1021/acs.analchem.6b01900. [PubMed: 27454138]

(57). Ricci F; Plaxco KW E-DNA sensors for convenient, label-free electrochemical detection of hybridization. Microchim. Acta 2008, 163 (3), 149–155. DOI: 10.1007/s00604-008-0015-4.

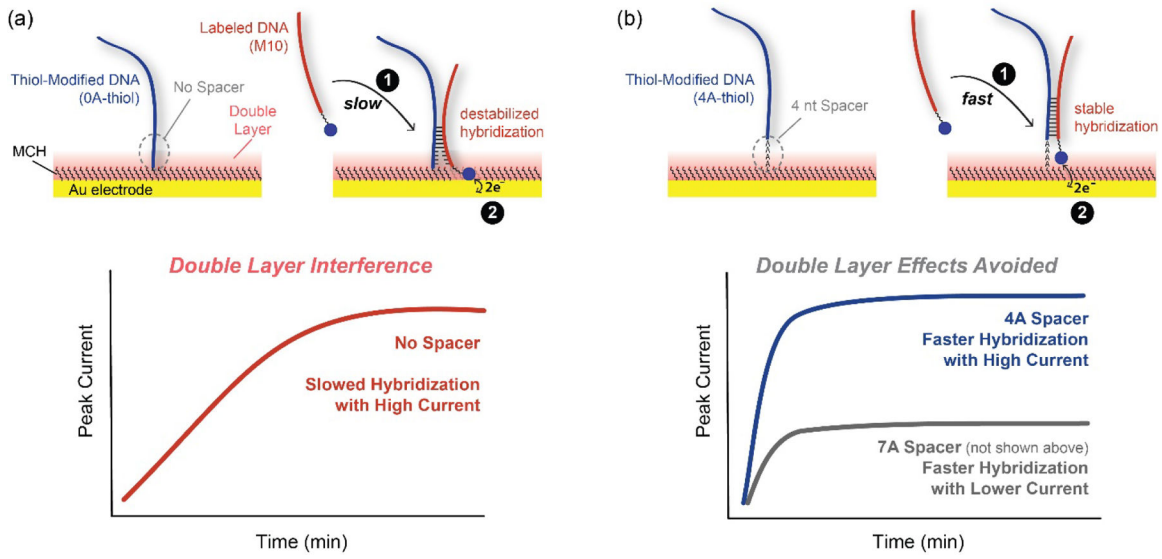

Figure 1.

Schematic representation of the sensor surface for studying DNA hybridization kinetics (short segments of 10 bp) at different sites relative to the electrode. The electrode surface is shown **(a)** without a spacer and **(b)** with an example poly-adenine (4 nt) spacer. Double-layer effects are shaded red. Mercaptohexanol (MCH) layer (~1.2 nm) is included, with thickness drawn roughly to scale compared to the double-layer at 0.5 M salt. Schematic depictions of the effects of double-layer interference on time-dependent SWV peak currents are shown at bottom. Numbered labels at top indicate that two convoluted processes will affect the measured current, DNA hybridization equilibria (1) and distance-dependent electron transfer (2).

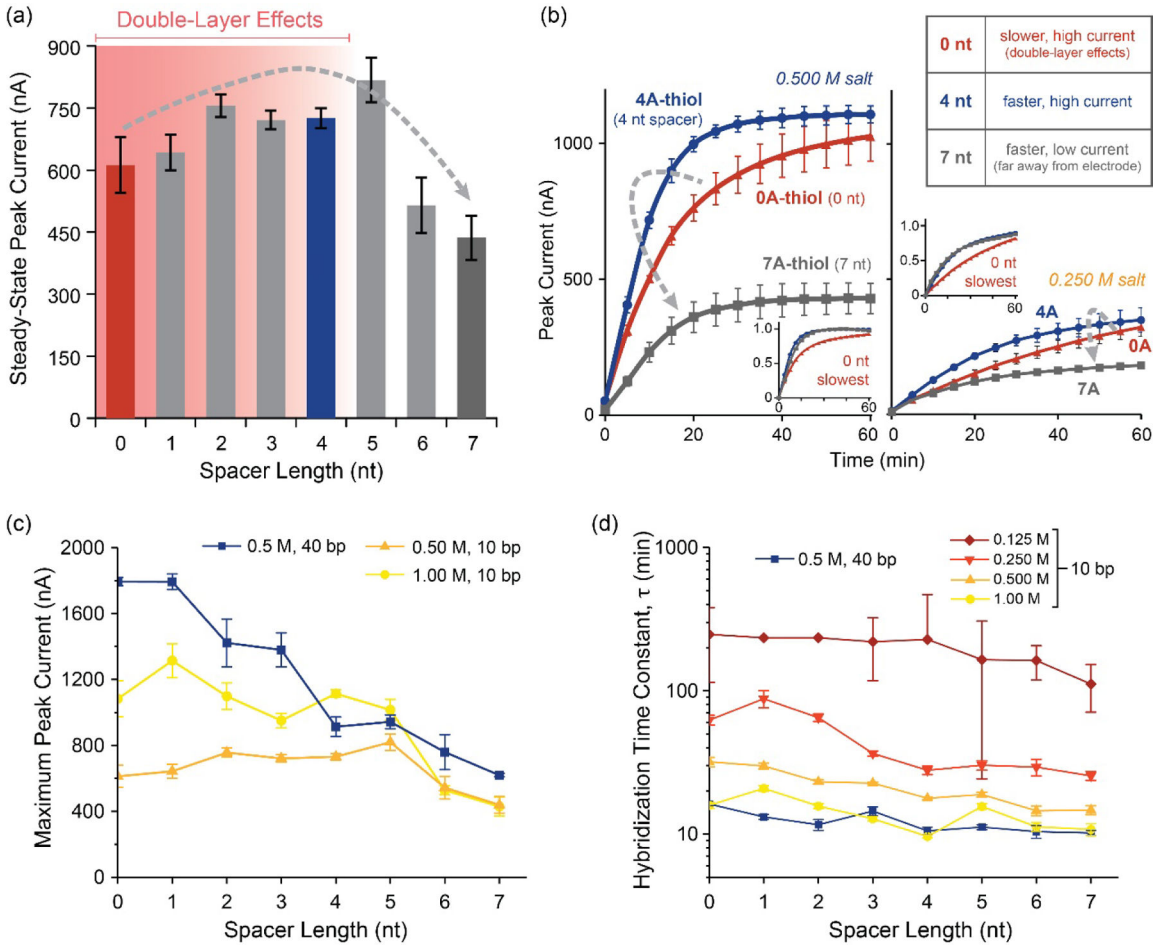

Figure 2.

DNA hybridization interference near the electrode surface was observed. **(a)** Steady-state peak currents were highest when the hybridized segment was at an intermediate distance from the electrode (4–5 nt). At longer distances (6–7 nt), current dropped in a predictable way. Closer to the electrode, a gradual but significant decrease in current was observed, likely from double-layer effects (shaded in red). **(b)** Hybridization kinetics of M10 DNA versus distance from the surface at 0.5 M salt (left) and 0.250 M salt (right). Hybridization was faster at intermediate (4 nt) and longer (7 nt) spacer lengths, while kinetics were slowed near the surface (0 nt; red). Insets show normalized data. More thorough studies of **(c)** peak current and **(d)** hybridization time constants at varying ionic strengths gave further evidence of interference near the electrode surface. The gray dashed arrows are included as visual aids to follow changes with increasing distance from the surface. Error bars depict standard deviation of triplicate electrodes.

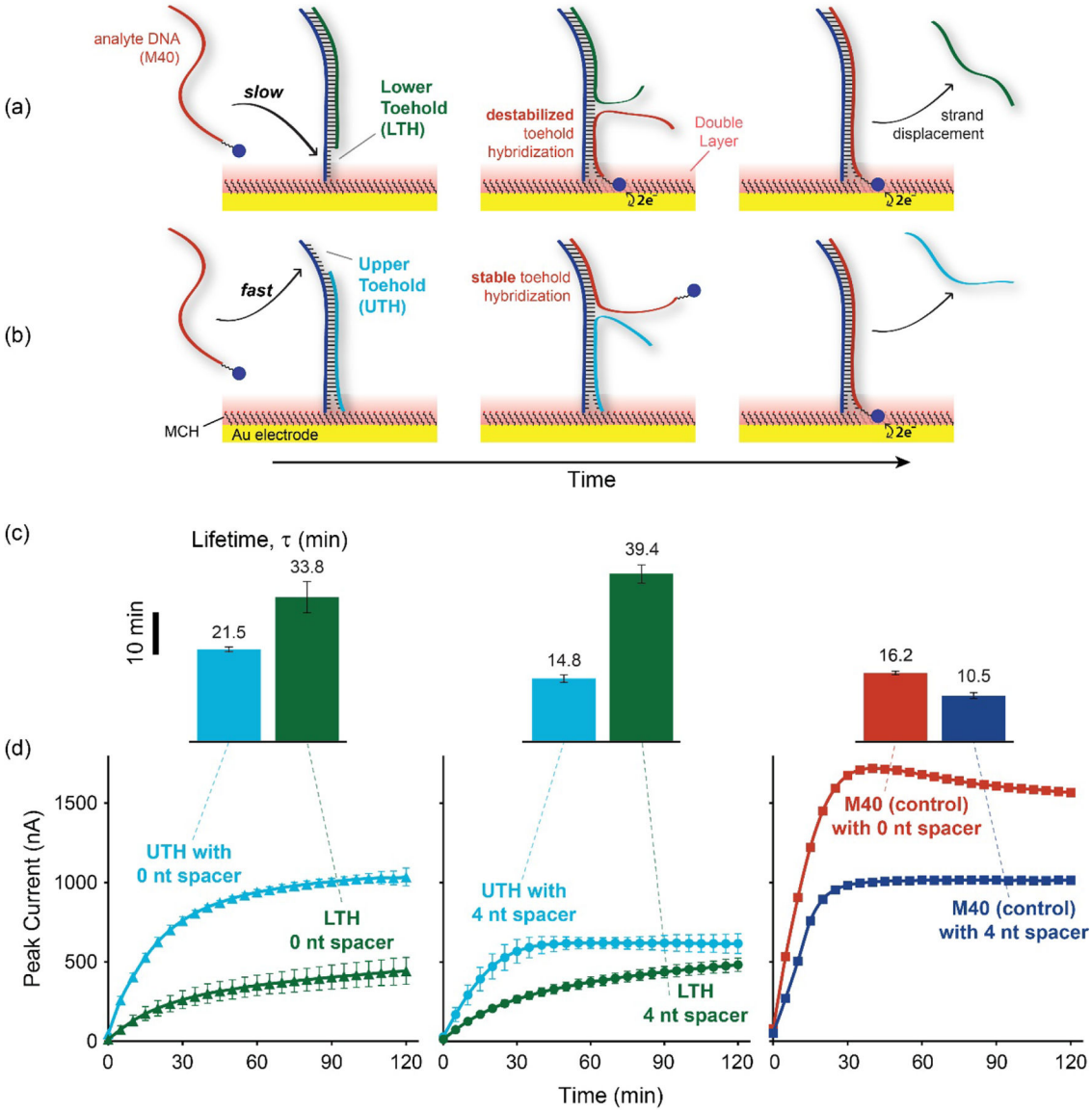

Figure 3.

Toehold mediated strand displacement on gold electrodes confirmed hybridization interference near the surface. **(a)** Lower toehold (LTH) system, destabilized by the double-layer, with slower hybridization. **(b)** Upper toehold (UTH) system permits fast hybridization. **(c)** Average hybridization time constants, **τ**, depicted in bar graphs color-coded to match kinetic data in **(d)**. **(d)** Kinetic data for the LTH, UTH, and control systems. M40 control experiments shown at right (red, blue). Experiments were done at 0.5 M ionic strength with three electrodes each; error bars depict standard deviation.

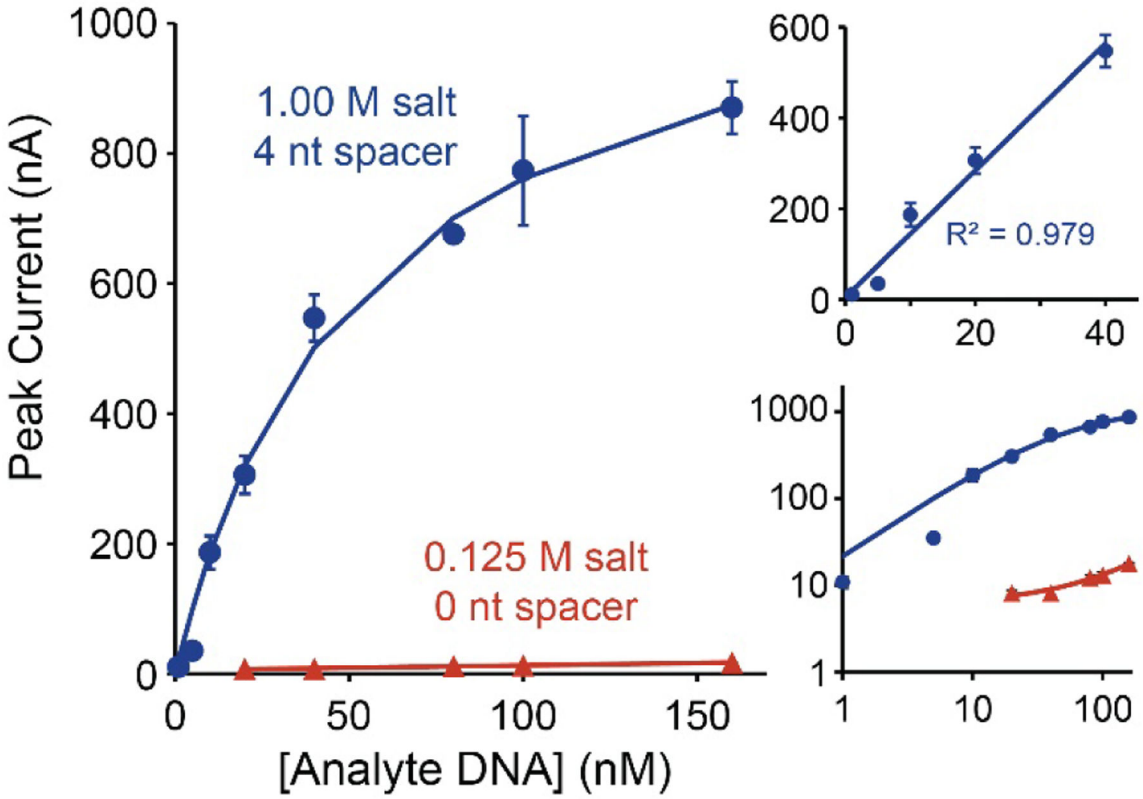

Figure 4.

EC-based DNA sensor under favorable (blue) and unfavorable (red) conditions. Favorable conditions (high ionic strength, 4 nt spacer) gave a ~190-fold sensitivity improvement and a ~130-fold LOD improvement (LOD = 300 pM). Inset plot at upper right shows the linear region; inset on lower right shows a log-log plot of the full curves.